CFD study of a horizontal axis wind turbine NREL Phase II

R. Belamadi [1,2*], R. Mdouki [2], A. Ilinca [3†] and A. Djemili [1]

[1] Mechanical of Materials and Industrial Maintenance Laboratory, LR3MI
Mechanical Engineering Department, Badji Mokhtar
University, Annaba, P.B. 12, Annaba 23000, Algeria

[2] Energy and Turbomachinery Laboratory, Mechanical Engineering Department
University of Tebessa, Tebessa, Constantine Road 12002, Algeria

[3] Wind Energy Research Laboratory, University of Québec at Rimouski 300
Allée des Ursulines, C.P. 3300 Rimouski, Québec, Canada G5L 3A1

(reçu le 20 Novembre 2015 – accepté le 28 Décembre 2015)

Abstract - The present work aims to study the aerodynamic characteristics of the NREL phase II (generated only with S809 profile along the span for an untwisted case) rotor that is a horizontal axis downwind wind turbine rotor and which is assumed to stand isolated in the space. The two dimensional steady-incompressible flow Reynolds average Navier-Stokes equations, are solved by using the commercial CFD package Ansys Fluent. The 2D computations are first performed on S809 airfoil in order to define the most suitable model to be used; the turbulence closure model has been chosen among four possible candidates (standard $k-\varepsilon$, Spalart-Allmaras, $k-\omega$ and $k-\omega$ sst) based on comparison of pressure coefficient for the different configurations with experimental results. Secondly, through a three dimensional study we tried to simulate the experiment for wind speed velocities of 7.2, 10.56, 12.85, 16.3, and 9.18 m/s. Results of pressure and torque for considered wind turbine rotor have been directly compared to the available experimental data. The comparisons show that CFD results along with the turbulence model used can predict the span-wise loading of the wind turbine rotor with reasonable agreement. The work presented here is the first stage of project that aims at giving a better understanding of the main influence of the rotational effect on boundary layer separation, and identify the stalled configuration in order to control this latter in future work.

Résumé – Le présent travail a pour objectif l'étude des caractéristiques aérodynamiques de la phase NREL II (générée juste avec un profil S809 tout au long de la durée pour un cas brut) d'un rotor vent arrière à axe horizontal d'un moteur d'éolienne et qui présume rester isolé dans l'espace. Les deux équations à deux dimensions Reynolds calculant la moyenne de Navier-Stokes d'un écoulement stable-incompressible sont résolues à l'aide du Pack commercial Ansys Fluent CFD. Les calculs 2D sont d'abord exécutés sur un profil aérodynamique S809 pour définir le modèle le plus approprié à être utiliser. Le modèle de fermeture de turbulence a été choisi parmi quatre choix possibles (Standard, Spalart-Allmaras, $k-\omega$ et $k-\omega$ sst) est basé sur la comparaison de coefficient de pression pour les configurations différentes avec les résultats expérimentaux. Deuxièmement, par une étude tridimensionnelle que nous avons essayé de simuler pour des vitesses de vent de 7.2, 10.56, 12.85, 16.3 et 9.18 m/s. Les résultats de pression et le moment de torsion pour le rotor d'éolienne considéré ont été directement comparés aux données expérimentales disponibles. Les comparaisons montrent que les résultats de CFD avec le modèle de turbulence utilisé peuvent prévoir le chargement d'envergure du rotor d'éolienne avec accord raisonnable. Le travail présenté est la première étape d'un projet qui vise à donner une meilleure compréhension de l'influence principale de l'effet rotatif sur la séparation de la couche de frontière et identifier la configuration calée pour contrôler ce dernier dans les futurs travaux.

Keywords: NREL phase II - Horizontal axis wind turbine – CFD.

* belamadi.riyadh@gmail.com , mdouki_ramzi@yahoo.fr
† adrian_ilinca@uqar.ca , djemili_abdelouheb@yahoo.fr

1. INTRODUCTION

Wind energy is becoming a significant contributor to the world's electrical energy generation systems and it is the fastest growing source of energy in the world today. Wind energy has become not only the renewable energy of choice, but also the least-cost option for new generation. Thousands of wind turbines are installed every year around the world and feed with electrical power the local or interconnected electricity grids. Numerical solution of flows through wind turbines is increasingly useful since it helps reduce time and cost in wind turbine development. The literature reports various methods that compare numerical predictions to experiments. The Blade-Element momentum Method [1] consists on dividing the flow in annular control volumes and applying momentum balance and energy conservation in each control volume. The method is indeed computationally cheap and thus very fast, even with providing very satisfactory results [2]. Actuator disc method, in this model the rotor is represented by a permeable disc that allows the flow to pass through the rotor. The classical actuator disc model is based on conservation of mass, momentum and energy, and constitutes the main ingredient in the 1D momentum theory, as originally formulated by Rankine and Froude [3]. Vortex lattice [4], lifting line, panel and vortex methods are also used to predict and design of wind turbine rotor. This list is far to be exhaustive.

The first applications of CFD to wings and rotor configurations were studied back in the late seventies and early eighties, in connection with aircraft wings and helicopter rotors, using potential flow solvers. In the field of aerodynamic research this technique has become increasingly important and it is prominent for studying turbo machinery. In this method the Navier-Stokes solver solves the governing equations of the flow directly. So it has the potential to predict the correct flow fields without a prior knowledge of the airfoil load characteristics. Natalino *et al.*, [5] used the RANS equation to solve the 3-D turbulent-steady incompressible flow of HAWT, the results show that the predicted values of the power generated are found to be in good agreement with those calculated with BEM method using the Spalart-Allmaras and the k-ω SST turbulence models for closure. The computational domain is discretized with a structured grid of near 1.5 million of volumes. Le Pape *et al.*, [6] based on the experimental results tested NREL in the NASA Ames large wind tunnel, several 2D and 3D Navier-Stokes computations performed with the compressible solver. The results of 2D computation show that the $k-\omega$ with the addition of SST correction gives the best results. Ideed the SST correction allows to detect the stall angle of the airfoil. According to the same authors for the 3D computation, the comparison torque with experiment shows good agreement at low wind speeds but important differences at high speeds. RANS solver was also used for prediction of aerodynamic loads on NREL Phase II, III and VI, the result showed an agreement with experimental results in [7-10]

The present work focuses on the numerical investigation of a three-bladed small-sized rotor from the Viscous and Aero elastic Effects on Wind Turbine Blades - Phase II project [11]. While a large amount of results can be extracted from this study, results will restrict to pressure and pressure coefficients distribution on the blade, generated torque and a general overview of the flow field around the rotor. Therefore, the flow model is three-dimensional, at steady state, incompressible regime and the flow-field is always assumed to be fully turbulent.

2. 2-D COMPUTATION

2.1 Airfoil description

The NREL S809 airfoil, illustrated in figure 1, is a 21 % thick airfoil specifically designed for HAWT applications. A 600 mm chord model of the S809 airfoil was tested in the 1.8 m × 1.25 m wind tunnel at the Delft University of Technology. The data from this experiment as reported by Somers [12] is used in this study for a Reynolds number

of $\mathrm{Re}=10^6$. The analysis of the test data and associated computational work highlights two main elements affecting airfoil performance: the laminar-turbulent transition and the turbulence modeling [13, 14].

Another wind tunnel campaign was performed at the Ohio State University on the S809 airfoil in a 1 m × 1.4 m wind tunnel [15], for different Reynolds numbers and different configurations (steady state/pitching oscillations, clean/rough surface), in order to further study the influence of these factors.

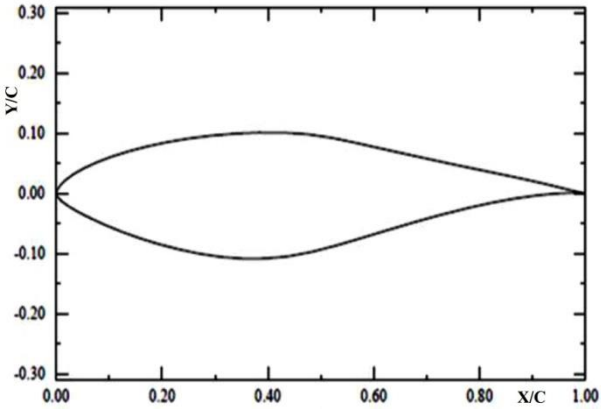

Fig. 1: NREL S809 airfoil geometry

2.2 Computational domain and grid

The computational domain is illustrated in figure 2. Velocity inlet boundary conditions are imposed for the inlet and the far-field and pressure outlet for the exit. Airfoil is treated as a stationary wall with no slip shear. The airfoil chord length is 600 mm [12]. The mesh consists of 60,000 quadrilateral cells, as shown in figure 2. The grid is C-type with 300 elements on the airfoil and in stream wise direction; the wake was modeled with 100 cells, 80 cells upstream and normal to the airfoil surface. A large number of grid points are near airfoil surface to accurately capture the gradients in the boundary layer.

The wall functions models need to adjust the thickness of neighboring cells to blade surface; a value of 0.00005 m is used for $k-\varepsilon$ standard wall functions and 0.00001m for the others models in order to satisfy $y+\geq 30$ and $y+\leq 1$ respectively, where $y+$ is the characteristic dimensionless distance from the wall. In the far-field area, the mesh resolution becomes progressively coarser since the flow gradients approach zero. This mesh size has been selected after grid independence analysis.

1.3 Results and analyses

The numerical solution is compared with experimental data to determine the turbulence model to be used and overall computational setup. Reynolds number was set at $\mathrm{Re}=10^6$ and flow speed is 48.68 m/s. Calculations are performed for two values of the angle of attack AoA, i.e. 14.24° and 20.15° and the pressure coefficient C_p has been compared with experimental results of Somers [12].

The pressure coefficient is defined as:

$$C_p = \frac{(P - P_\infty)}{1/2\,\rho.V^2}$$

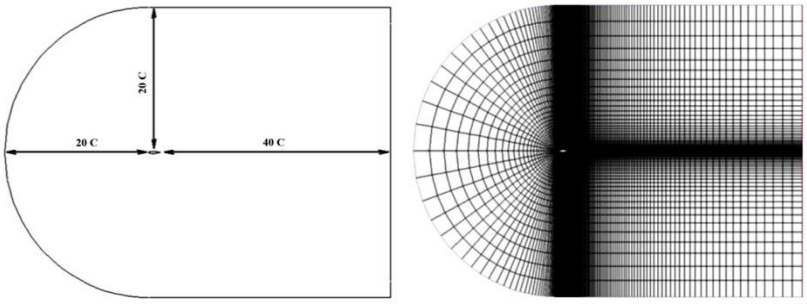

Fig. 2: Computational domain & Structured CH-type mesh

Where P is the local static pressure on the blade surface; P_∞ is the static pressure and $1/2\ \rho.V^2$ is the dynamic pressure of the free stream.

In figures 3 and 4, the computed pressure distribution on airfoil surface is compared with experimental data for angles of attack AoA = 14.24° and 20.15°, respectively. The C_p comparisons for 14.24° show reasonably good agreement over the entire airfoil surface for all turbulence models, except near the leading edge (LE) for $k-\omega$ standard model.

The experimental data show that separation occurs at 50 % of the chord on the upper surface for an AoA of 14.24°. The calculations predict the separation slightly later. At an angle of attack AoA = 20.15°, an early separation (15-20 % of the chord) is identified in experimental data, where pressure coefficient flattens. The calculations predict separation only at approximately 30 % of the chord.

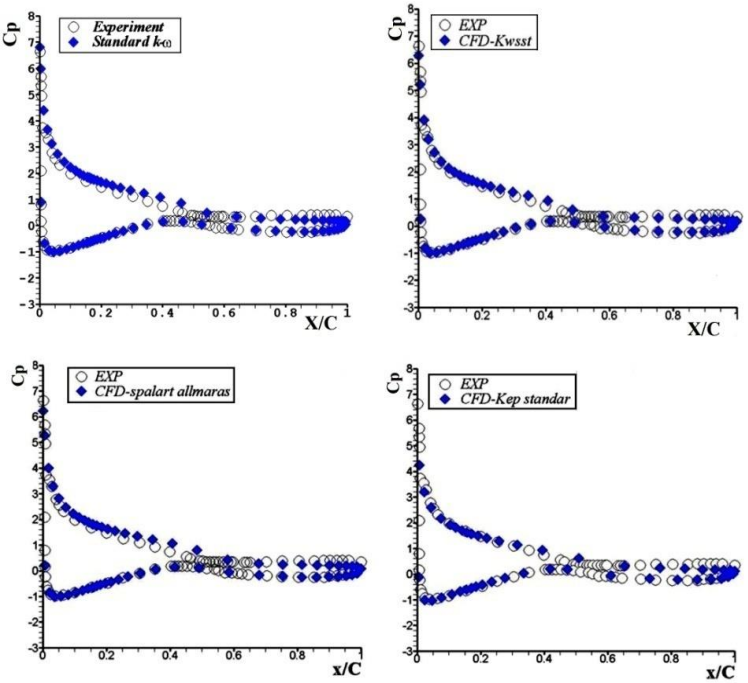

Fig. 3: Comparison of numerical and experimental results [21] for pressure coefficient distribution at AoA = 14.24°

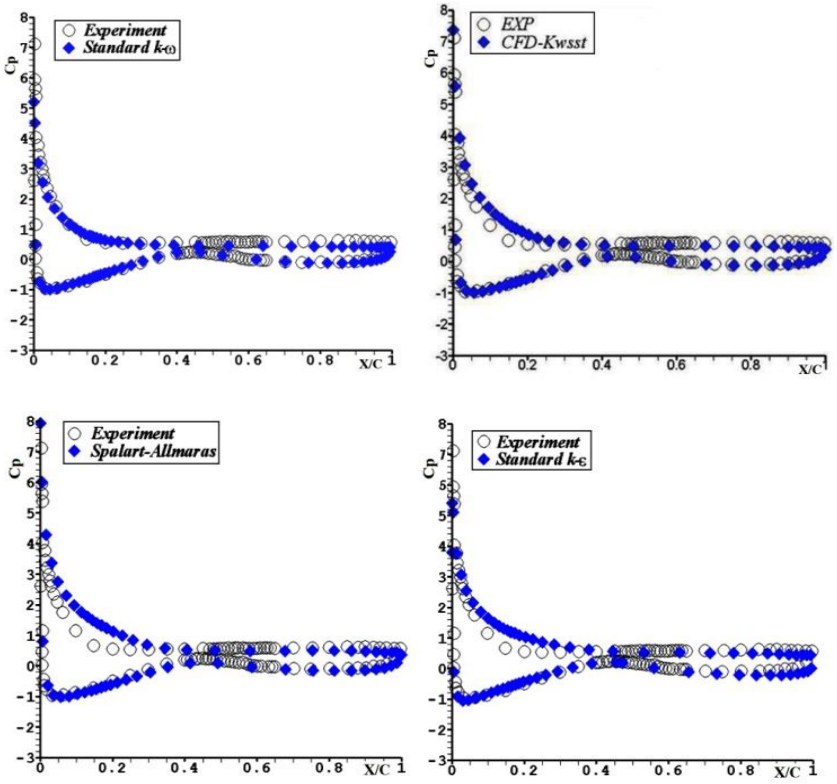

Fig. 4: Comparison of numerical and experimental results [21] for pressure coefficient distribution at AoA = 20.15°

The computed pressure distribution agrees well with the experiment except for small differences over the first 20 % of the chord, and this for all turbulence models.

These first computations show that all these models are good candidates for the turbulence modeling, especially the $k-\omega$ with standard wall function and $k-\omega$ SST. For the following computations we are choosing $k-\omega$ with SST correction model.

3. 3-D COMPUTATION

3.1 Turbine geometry

The experimental data for NREL Phase II is obtained from the IEA Annex XIV database [11]. This database was built as a contribution of many European research labs and the NREL to store and document the experimental data for various tested wind turbines and make it available to researchers. NREL phase-II rotor mounted on a downwind machine is a small three bladed HAWT rotor with 5.029 m radius [16], as shown in figure 5. The blades of the phase-II rotor are non-twisted and non-tapered with a constant cord of 0.4572 m. The NREL S809 airfoil series is used, except for the root. At 14.4 % span the airfoil thickness is $t/c = 20.95\%$ and decreases linearly to $t/c = 20.95\%$ at 30 % span, while outboard of 30 %, thickness is constant at that value. The nominal rotation speed is 71.68 rpm and the pitch is 12 deg.

Fig. 5: NREL Phase II Rotor

3.2 Computational domain and grid

At the initial stages of the project, efforts were focused on trying to create a different mesh cells and type; structured, unstructured, C-type and H-type. Due to its advantage, it was decided to create a structured H-type mesh. Therefore increasing the grid generation times.

It also has to be noted that although the rotor is featured with three blades, only one blade is actually being treated by exploiting the 120 degrees periodicity of the three-bladed rotor Figure 5. The wind turbine tower and the ground effect were neglected; the computational domain is enclosed between a small inner cylinder where Euler-slip wall boundary condition was imposed and an outer cylinder with a symmetry boundary condition, the length of the radius of the domain equal to 3 times the rotor diameter (R) to eliminate far field effects.

The inlet was placed at $2R$ upstream of the blade where a uniform wind speed was assumed as velocity inlet boundary condition. Turbulence conditions also have to be defined here with the fixed value of turbulent intensity and viscosity ratio. Pressure outlet boundary condition was applied at $10R$ on the downstream direction of the rotor and sets the pressure at the boundary at a specific static pressure value.

In this study, the obvious choice was to put the value equal to zero so that the pressure at the outlet would be equal to the atmospheric operating pressure.

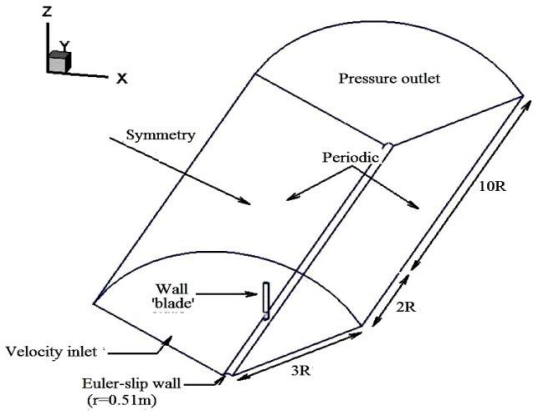

Fig. 6: One third-cylindrical domain and boundary condition

As shown in figure 6, the solution have been done for only one third domain include one blade, and use periodic boundary condition in order to account for all three blades with full domain. A hexahedral mesh of approximately 3.5 million cells (255 × 168 × 75 in x, y and z respectively) was generating. The thickness of the first cell to the wall was kept at 0.00002 m so that the $y+$ value falls between 1 and 5 which is suitable for $k-\omega$ with SST correction model.

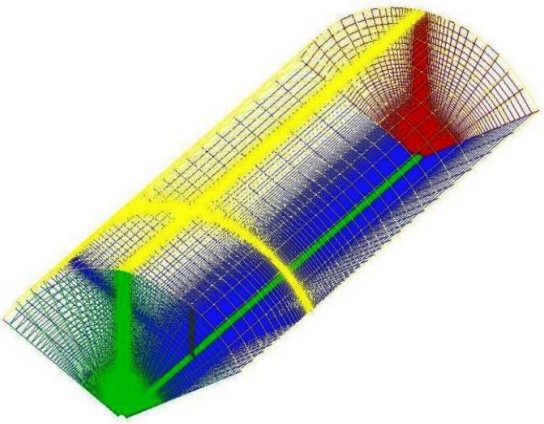

3D mesh

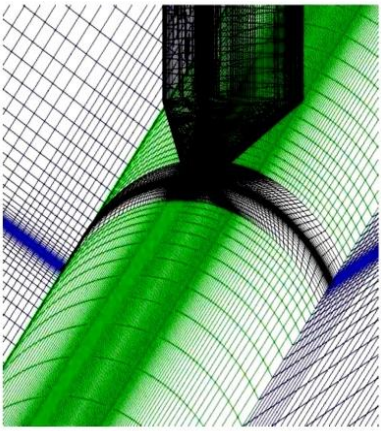

Bladeroot and hub

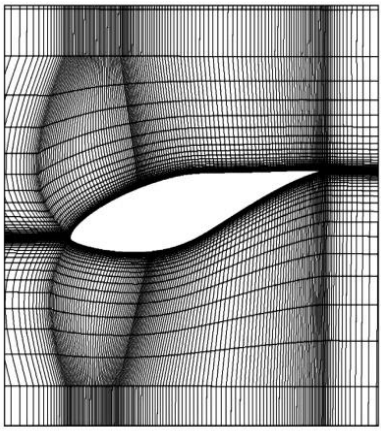

Leading and training edges

Fig. 7: Structured H-type mesh of One third-cylindrical domain

3.3 Solution method

The equations of fluid flow are usually solved by Fluent in a stationary reference frame. However, there are many problems that require the equations be solved in a moving reference frame. A rotating rotor of a wind turbine is such case. The one used here is called single moving reference frame (SRF). This latter permits an unsteady problem respect to the absolute reference frame to become steady in respect to the moving reference frame figure 8. In simple words, the whole computational domain is assumed to be rotating at the angular velocity of the turbine rotor [17]. This particular method is well suited for this problem since there is only one rotating wall.

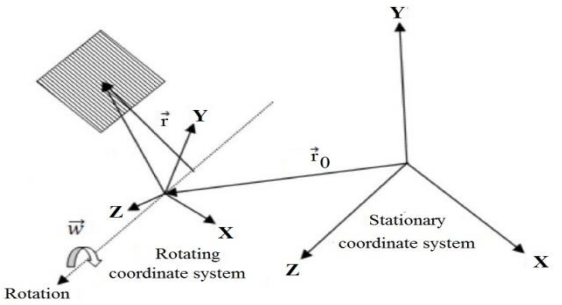

Fig. 8: Rotating, Frames, in view of stationary, Frames [17]

The fluid velocities can be transformed from stationary frame to rotating frame in respect with flowing equations:

$$\overrightarrow{V_r} = \vec{V} - \overrightarrow{U_r} \tag{2}$$

where

$$\overrightarrow{U_r} = \vec{\omega} \times \vec{r} \tag{3}$$

here, $\overrightarrow{V_r}$ is the relative velocity (viewed from rotating frame), $\vec{V}$ is the absolute velocity (viewed from stationary frame), and $\overrightarrow{U_r}$ is the whirl velocity due to the rotating coordinate system.

The pressure-based discretization scheme is being applied with coupled algorithm, which solves in one step the system of momentum and pressure-based continuity equation. The solution was initialized with first-order upwind discretization scheme for all variables; pressure, momentum and turbulence equations, when some convergence is achieved, it can switch to second-order. This is done in order to limit convergence problem. The number of iterations adjusted to reduce the scaled residual below the value of 10^{-5} which is the criterion of convergence. For each run, the observations of the static pressure, lift and drag coefficient were appointed for the convergence of the solution.

The three-dimensional steady state RANS equations are solved using Ansys-Fluent; the closure turbulence model is $k-\omega$ SST.

3.4 Results

The quantity and type of results that can be extracted from this type of numerical study is large, starting from integral aerodynamics, to pressure distribution and up to including wake study. Provided the aim of this study, results will restrict to pressure and pressure distribution on the blade, generated torque and a general overview of the flow field around the rotor. The numerical pressure distribution is presented and compared with experimental results at 30, 47, 63 and 80 % span wise locations for wind speed 7.2, 12.9 and 19.18 m/s.

At 7.2 m/s, the computed pressure distribution at all sections of the blade is in good agreement with the experimental data (figure 9). At this wind speed, the flow is completely attached and no separation occurs except up to 30 % span, where flow is separated on 30 % chord length and we observe some deviation that is due to a known difficulty of RANS turbulence models in solving separated flow.

At 12.85 m/s, important discrepancies between the computed and experimental pressure distribution in the suction side are observed in the $r/R = 0.30$ section near the blade root (figure 9). Disagreement seems to increase with wind speed and especially for the suction side of the blade, at this speed a stronger vortices were formed close to the root. That is the reason behind such discrepancy.

At 19.18 m/s, again there is an important discrepancy at section $r/R = 0.30$ in the suction side. At $r/R = 0.8$ we observe a disagreement with the experimental result near to leading edge in the suction side as shown in figure 10. At this speed, due to the stronger vortices formed at the root and the tip of blade it's very difficult to capturing the separation characteristic using RANS turbulence models.

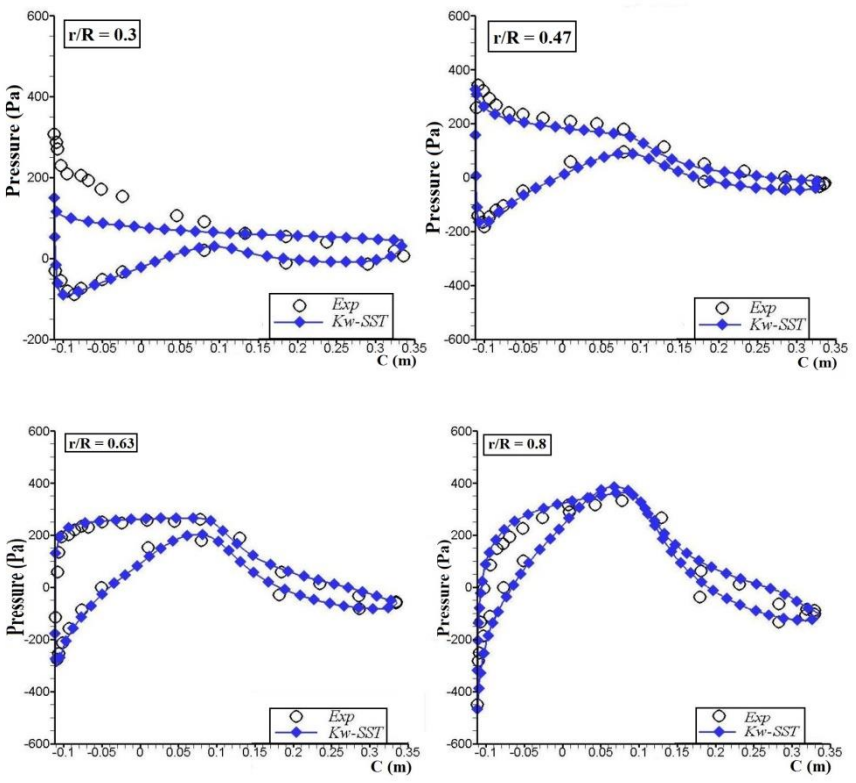

Fig. 8: Pressure distribution comparison between experimental and calculated at different span wise sections at 7.2 m/s for NREL II

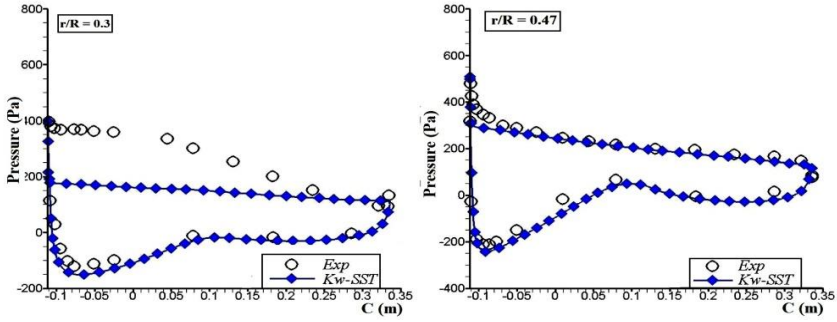

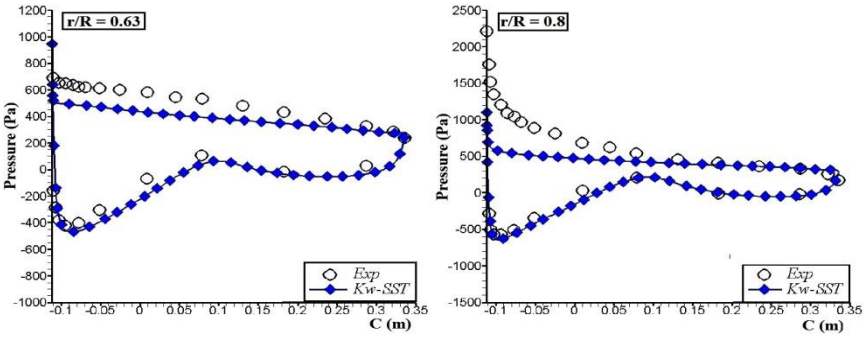

Fig. 9: Pressure distribution comparison between experimental and calculated at different span wise sections at 12.85 m/s for NREL II

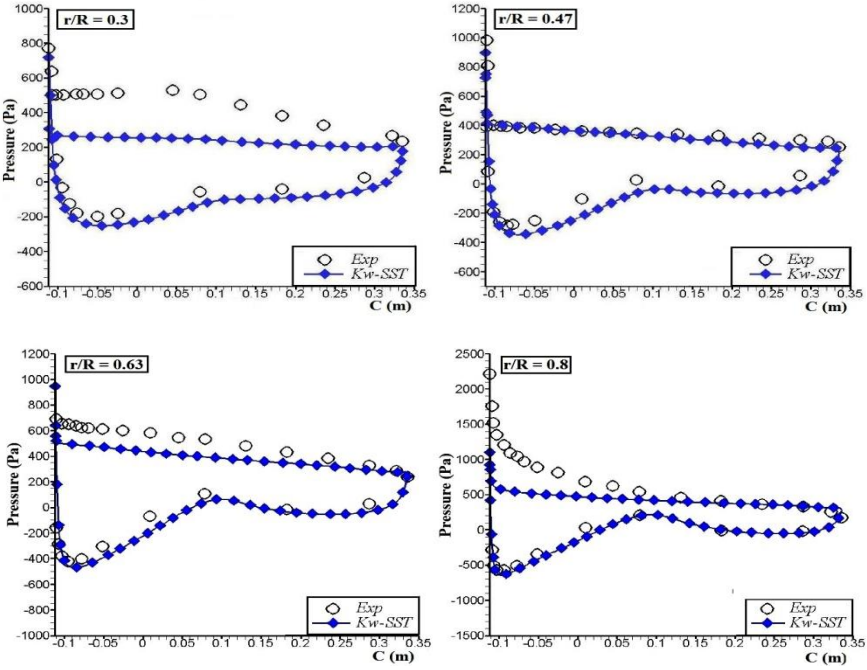

Fig. 10: Pressure distribution comparison between experimental and calculated at different span wise sections at 19.18 m/s for NREL II

Since the relative velocity magnitude gives a more information for airfoil aerodynamics, the separation is investigated by plotting the streamlines and contour of relative velocity magnitude at different span wise blade sections. The plots were obtained for wind speeds of 7.2, 12.85 and 19.18 m/s.

In figure 10-**a.b**- can be observed that at 7.2 m/s the flow is attached on most of the blade surface except for small regions at $r/R = 0.3$. The results obtained support the previous discussion (figure 8), where the pressure distribution in good agreement with experimental results.

At 12.85 m/s, the results give more precise information figure 11 -a.b-; it can be observed that the separation with tow vortices occur at r/R=0.3 on the suction side. The vortices decrease to one vortex at $r/R = 0.47$ and vanishes at $r/R = 0.63$ and

$r/R = 0.80$ .Again, the results obtained support the previous discussion (figure 9). The discrepancy in pressure distribution also decreases as one goes from root to tip.

At 19.11 m/s. the separation effects are magnified at all blade sections (figure 12-a.b-), this explain the deviation of computed pressure distribution from experimental results of those sections (figure 10).

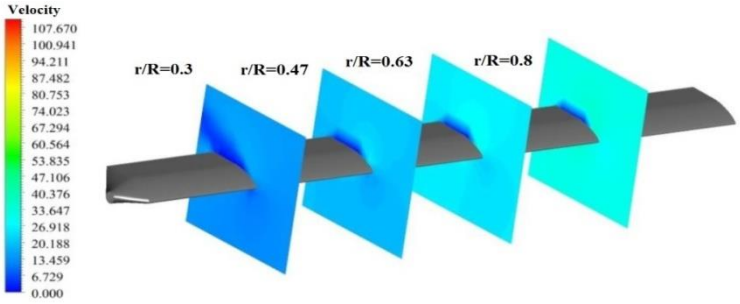

Fig. 11**a-**: Contours of velocity magnitude for all radial stations at 7.2 m/s

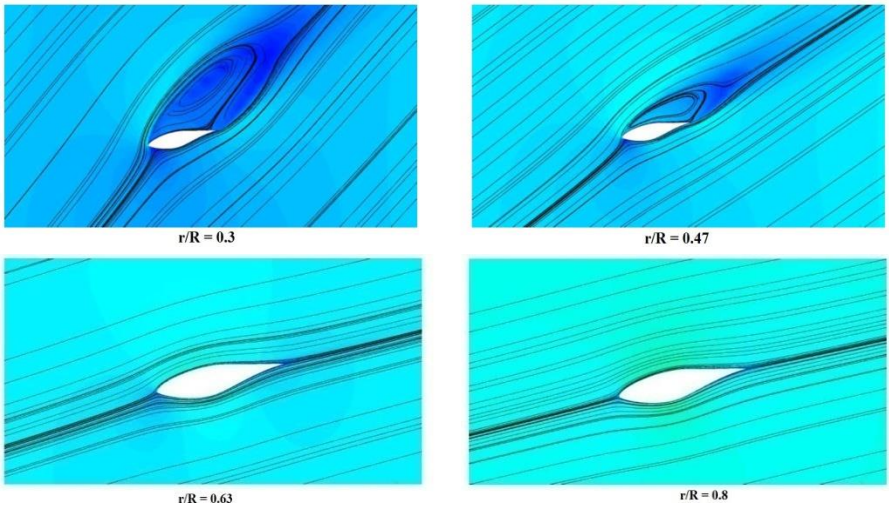

Fig. 11**b-**: Relative velocity contour with stream lines at 7.2 m/s on different section for NREL Phase II

To give more precise information, the development of the limiting streamlines with static pressure contour for both blade sides is shown in figure 13. At 7.2 m/s can be observed that on suction side the separation starting from the root to $r/R = 0.3$, due to the strong 3D effects near to the blade root. At 12.85 m/s separation seems to be widely experienced at $r/R = 0.8$ of the blade, while the separation occupy most of the suction side at 19.18 m/s except for a small area near to the blade tip. On a rotating blade there's two main forces play an important role in separated boundary layer, i.e. the centrifugal forces that produce a span wise pumping effect that leads to the deviation of the streamlines in span wise direction towards to the tip. On the other hand, Coriolis force, which acts in the chord wise direction as a favorable pressure gradient that tends to deay separation.

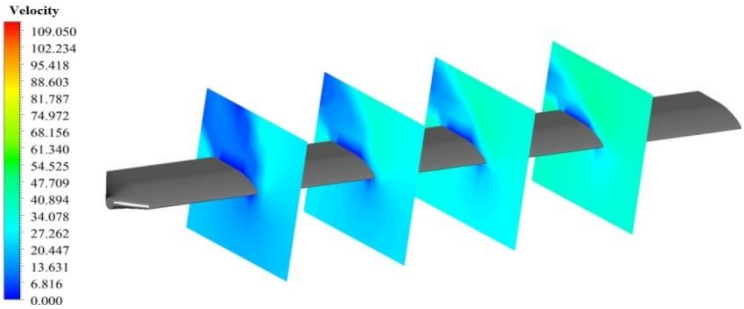

Fig. 12**a-**: Relative velocity contour for all radial stations at 12.85 m/s

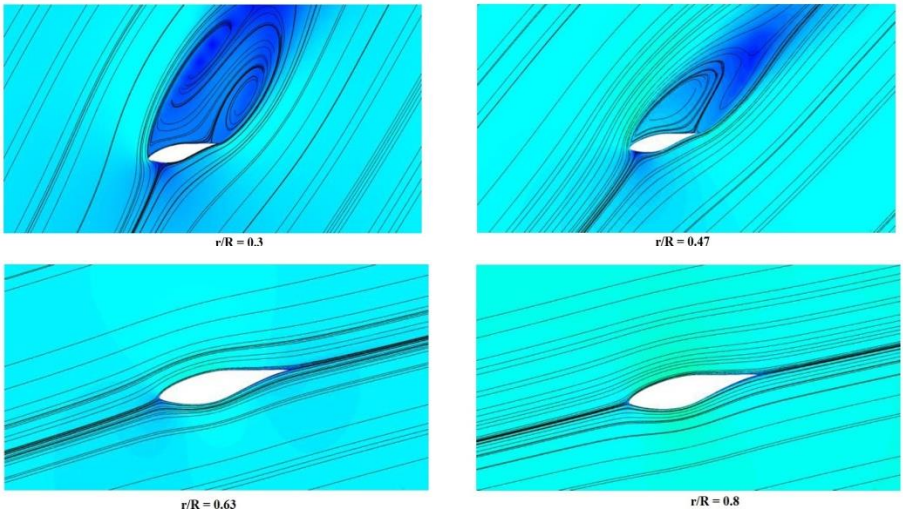

Fig. 12**b-**: Relative velocity contour with stream lines at 12.85 m/s in different section for NREL Phase II

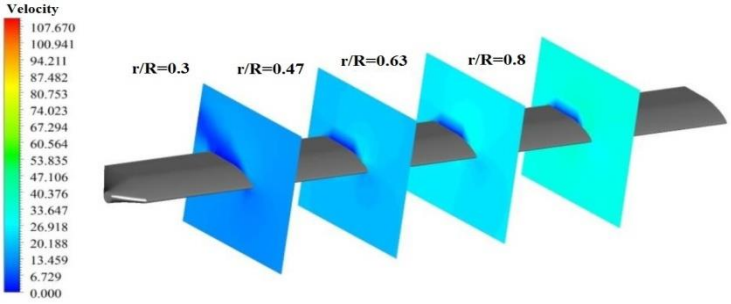

Fig. 13**a-**: Contours of velocity magnitude for all radial stations at 19.18 m/s

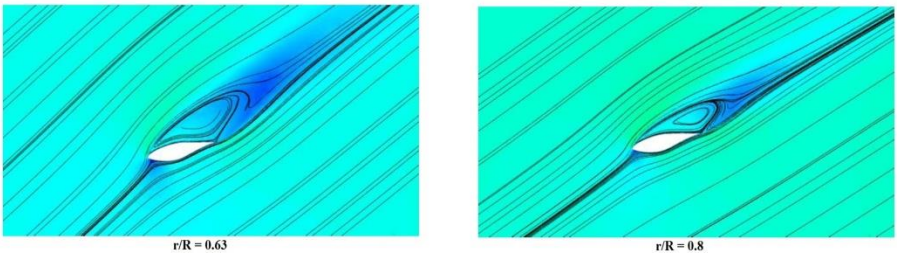

Fig. 13**b-**: Relative velocity contour with stream lines at 19.18 m/s on different section for NREL Phase II

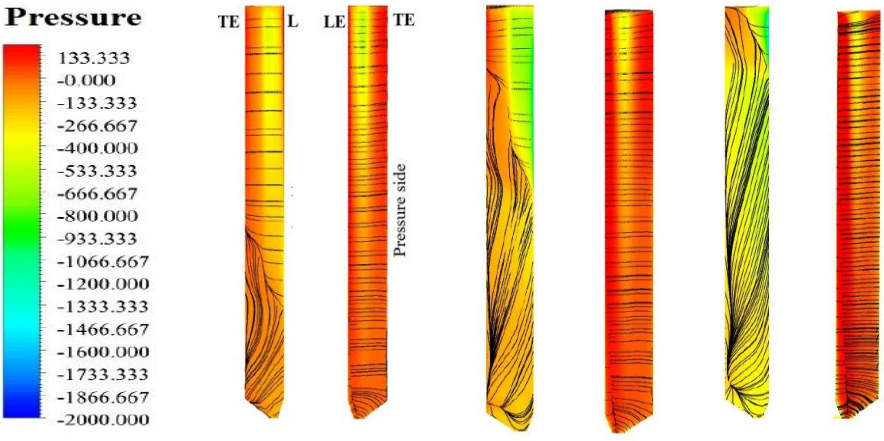

Fig. 14: Limiting stream lines with static Pressure of NREL Phase II compared with numerical result [18]

The comparisons of rotor torques are shown in **Table 2**. At 7.2 m/s the computed torque has a good agreement with strain gauge measurement than with the generator measurement; while at 10.56 m/s the trend is reversed. This is perhaps due to the fact that at low wind speed the blade flapping is low, thus the strain gauge measurement is accurate while the generator correlation is not accurate in this region because it is far from it design operating condition [19]. More the speed increases the blade flapping become stronger while the generator gets closer to its design operating range, hence the reverse.

Table 1: Torque prediction errors at Wind speed 7.2 & 10.56 m/s for NREL II

Wind speed (m/s)	CFD	Experiment			
		Strain gauge		Generator	
	Torque (Nm)	Torque (Nm)	Error (%)	Torque (Nm)	Error (%)
7.2	29051	289.22	1.49	317.26	-8.43
10.56	1088.56	1207.39	-9.84	1190.04	-8.52

In comparing the rotor torque derived power against the generator power, it was found that the efficiency did not match the published efficiency. As a result, a better curve fit between mechanical and generator power was found in [20], as described below:

$$P_{Generator} = 0.9036\ P_{Mechanical} - 0.847$$

The computed power as a function of the wind speed is showed in figure 15 against the experimental IEA data [11], numerical results of Aerodyn/Yawdyn by Duque *et al.* [20] and BEM results by Ceyhan *et al.* [21]. For the computed power results, the mechanical power was corrected to generator power using equation (4). The CFD results are found to be in good agreement with those obtained using the BEM method and measured one, for the tested undisturbed wind speed, ranging from 7.2 to 12.83 $m.s^{-1}$ for generally attached flow conditions. In fact at 10.56 m/s, the predicted power is1.80 % lower than measured one; more the wind speed increase the predicting power error increases, at 12.83, 16.3 and 19.18 m/s the predicted power is 5.22, 20.36 and 28.19 % lower than measured one respectively. The results show considerable differences however at the higher wind speeds and in predicting maximum power. For deep stall conditions, the lack of the RANS models capabilities in predicting the aerodynamic loads is well-known.

Figure 16 shows a comparison of the measured and computed power coefficients for various wind speeds and tip speed ratio. It is interesting to note that the CFD computation performed with Fluent have a similar trend with measured one and the others numerical results; It is noticeable that the maximum computed value of power coefficient is only about 0.15, achieved at wind speed of 10.56 m/s and tip speed ratio 3.59. The value is much less than the Betz limit (0.593).To date, no wind turbine has been designed which is capable of exceeding this limit. The power coefficient of wind turbines currently in operation is lower than 0.593 and that of the recently commercialized small- or middle-sized wind turbine is around 0.45 [22]. At the lower tip speed ratios and the higher wind speed is the stall that plays a major role, in reducing the overall aerodynamic efficiency.

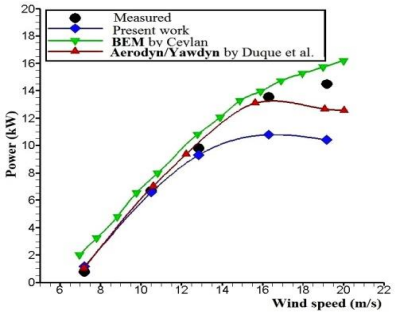

Fig. 15: Variation of experimental (NREL Phase II) and computational power output as function of windspeed

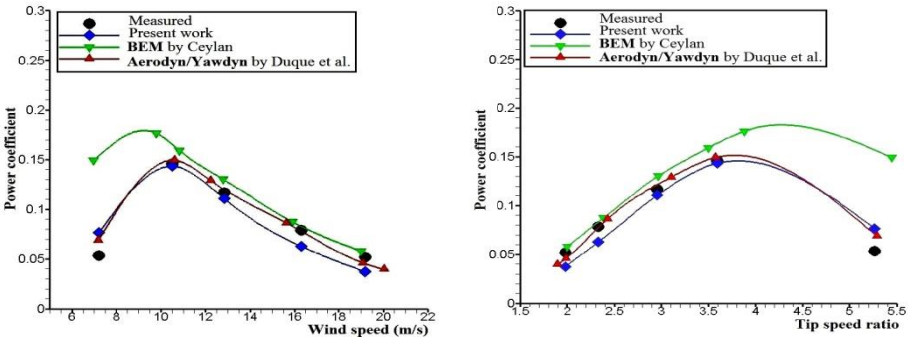

Fig. 16: Variation of experimental and computational power coefficient as function of wind speed(left) & tip speed ratio (right).

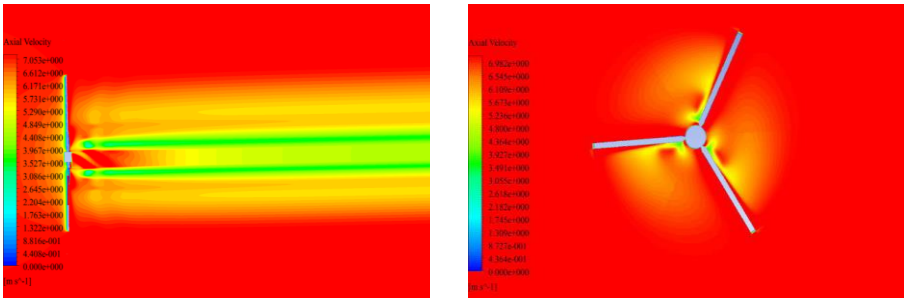

At 7.2 m/s

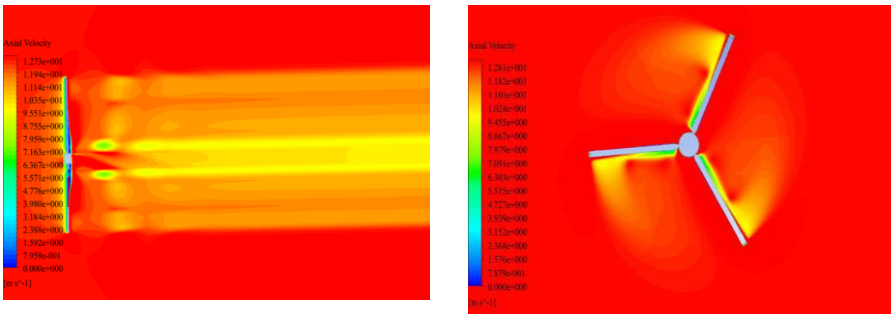

At 12.85 m/s

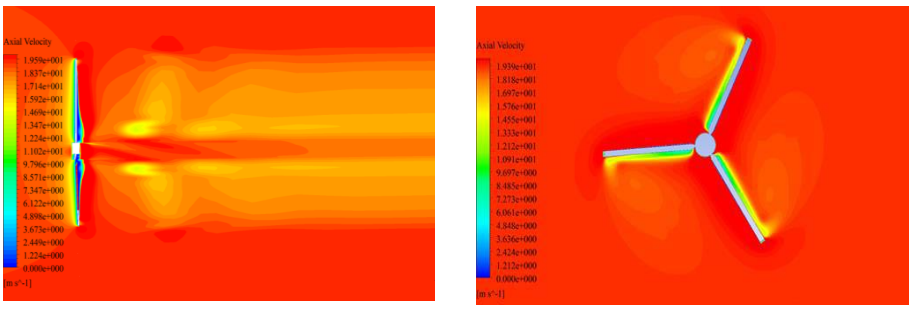

At 19.18 m/s

Fig. 17: Near wake axial velocity distributions (left) &Contour of axial velocity in wake sections (right)

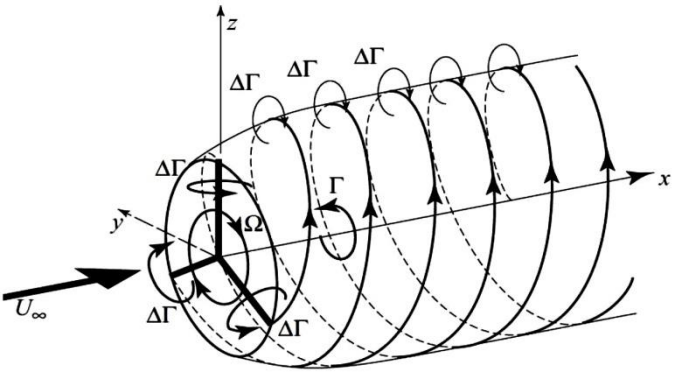

Fig. 18: Scheme of the helical wake of a HAWT [23]

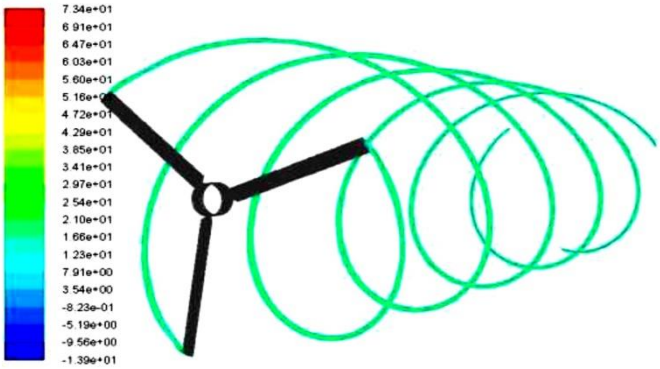

Fig. 19: Path lines at blade tip colored with the axial velocity component, at 19.18 m/s

3. CONCLUSION

The aims of the current works is the numerical study of HAWT rotor NREL Phase ii; the validation of the computed results with experimental data has been done. The results were restricting to pressure and pressure distribution on the blade, generated torque and a general overview of the flow field around the rotor. The numerical pressure distribution is presented and compared with experimental results at 30, 47, 63 and 80% span ise locations for wind speed 7.2, 12.9 and 19.18 m/s. When the flow is completely attached and no separation occurs the computed pressure distribution at all sections of the blade is in good agreement with the experimental data except up to 30% span, the disagreement seems to increase with wind speed and especially for the suction side of the blade, at this speed a stronger vortices were formed close to the root. That is the reason behind such discrepancy.

The computed torque has a good agreement with strain gauge measurement than with the generator measurement at wind speed 7.2 m/s; while at 10.5 6m/s the trend is reversed. The CFD results of power coefficient are found to be in good agreement with those obtained using the BEM method and measured one, for the tested undisturbed wind speed. The maximum computed value of power coefficient is only about 0.15, achieved at wind speed of 10.56 m/s and tip speed ratio 3.59. The results of power show considerable differences however at the higher wind speeds and in predicting maximum power. For deep stall conditions, the lack of the RANS models capabilities in predicting the aerodynamic loads is well-known.

The study confirms that RANS simulations are capable to solve with a fair accuracy the different aspects involved in HAWT flow field, thus this confirms that nowadays CFD simulations can be the most important tool for analysis and design of wind turbine rotors.

Acknowledgement - All computations have been carried out with the computer code ANSYS Fluent 15.0 at the 'Centre de Développement des Energies Renouvelables', (CDER, Algérie). The helpful assistance and comments of Dr O. Guerri from CDER are acknowledged with thanks.

REFERENCES

[1] J.N. Sorensen and W.Z. Shen, '*Numerical Modeling Of Wind Turbine Wakes*', Journal of Fluid Engineering, Vol. 124, pp. 393 - 399, 2002.

[2] E. Hau, '*Wind Turbines*', Springer-Verlag Berlin Heidelberg, 2000.

[3] C.E. Carcangiu, '*CFD-RANS Study of Horizontal Axis Wind Turbine*', PhD Thesis, Gagliari, Italia, 2008.

[4] F.J. Simoes and J.M.R. Graham, '*Application of a Free Vortex wake Model to a Horizontal Axis Wind Turbine*', Proceedings of 12th British Wind Energy Association Conference, pp. 161–165, 1990.

[5] N. Mandas, '*Numerical Prediction of Horizontal Wind Turbine Flow*', Department of Mechanical Engineering, University of Cagliari, Italia.

[6] A. le Pape and J. Lecanu. '3*D Navier-Stokes Computations of a Stall-Regulated Wind Turbine*', Wind Energy, Vol. 7, N°4, pp. 309 – 324, 2004.

[7] A. Gupta, '*Prediction of Aerodynamic Forces on Wind Turbine Blades using Computational Fluid Dynamics*', Master Thesis, Applied Science Industrial Systems Engineering, University of Regina, Italia, 2007.

[8] M. Ali El Farra, '*Horizontal Axis Wind Turbine Rotor Blade: Winglet and Twist Aerodynamic Design and Optimization Using CFD*', PhD Thesis, in Aerospace Engineering, Medal East technical University, 2011.

[9] F. Malatesta, '*CFD Study of Wind Turbine Rotor*', School of Engineering and Materials Science Third Year Project DEN 318, 2012.

[10] J.G. Schepers, A.J. Brand, A. Bruining, J.M.R. Graham, M.M. Hand, D.G. Infield, H.A. Madsen, R.J.H. Paynter and D.A. Simms, '*Final Report of IEA Annex XIV: Field Rotor Aerodynamics*', ECNC-97-027, Energy Research Center of the Netherlands, 1997.

[11] D.M. Somers, '*Design and Experimental Results for the S809 Airfoil*', Airfoil, State College, Pennsylvania, 1989.

[12] E. Sagol, M. Reggio and A. Ilinca, '*Assessment of Two-Equation Turbulence Models and Validation of the Performance Characteristics of an Experimental Wind Turbine by CFD*', International Scholarly Research Notices, ISRN Mechanical Engineering, Volume 2012, Article ID 428671, 10 p., 2012.

[13] F. Villalpando, M. Reggio and A. Ilinca, '*Assessment of Turbulence Models for Flow Simulation around a Wind Turbine Airfoil*', Modelling and Simulation in Engineering, paper #714416, 2011.

[14] R.R. Ramsey, M.J. Hoffman and G.M. Gregorek, '*Effects of Grit Roughness and Pitch Oscillations on the S809 Airfoil*', NREL N°TP-442-7817, December 1995.

[15] D. Simms, S. Schreck, M. Hand and L. Fingersh, '*NREL Unsteady Aerodynamics Experiment in the NASA-Ames Wind Tunnel: A Comparison of Predictions to Measurements*', National Renewable Energy Laboratory, NREL/TP-500-29494, 2001.

[16] ANSYS Inc., '*Ansys Fluent Theory Guide*', November 2010.

[17] N.N. Sorensen and J.A. Michelsen, '*Aerodynamic Predictions for the Unsteady Aerodynamics Experiment Phase II Rotor at the National Renewable Energy Laboratory*', AIAA-2000-0037, 2000.

[18] C. Thumthae and T.Chitsomboon, '*Optimal Angle of Attack for Untwisted Blade Wind Turbine*', Renewable Energy, Vol. 34, N°5, pp. 1279 – 1284, 2009.

[19] Earl P.N. Duque, W. Johnson, C.P. vanDam , R. Cortes and K. Yee, '*Numerical Predictions of Wind Turbine Power and Aerodynamic Loads for the NREL Phase II Combined Experiment Rotor*', AIAA-2000-0038, 2000.

[20] X. Chen and R. Agarwal, '*Assessment of the Performance of Various Airfoil Sections on Power Generation from a Wind Turbine Using the Blade Element Momentum Theory*', IJEE, Vol. 4, N°5, pp. 835 - 850, 2013.

[21] J.-Oh Mo and Y.-Ho Lee, '*CFD Investigation on the Aerodynamic Characteristics of a Small-Sized Wind Turbine of NREL Phase VI Operating with a Stall-Regulated Method*'', Journal of Mechanical Science and Technology, Vol. 26, N°1, pp. 81 - 92, 2012.

[22] T. Burton, D. Sharpe, N. Jenkins and E. Bossanyi, '*Wind Energy Handbook*', John Wiley & Sons Ltd: Chichester, 2001.